MONTE CARLO MODELING OF A VARIAN 2100C 18 MV MEGAVOLTAGE PHOTON BEAM AND SUBSEQUENT DOSE DELIVERY USING MCNP5

A Thesis
Presented to
The Academic Faculty

by

Jared Hoover

In Partial Fulfillment
of the Requirements for the Degree
Master of Science in the
George W. Woodruff School of Mechanical Engineering

Georgia Institute of Technology
August 2007

MONTE CARLO MODELING OF A VARIAN 2100C 18 MV MEGAVOLTAGE PHOTON BEAM AND SUBSEQUENT DOSE DELIVERY USING MCNP5

Approved by:

Dr. Farzad Rahnema, Advisor
School of Nuclear and Radiological Engineering
Georgia Institute of Technology

Dr. Chris Wang
School of School of Nuclear and Radiological Engineering
Georgia Institute of Technology

Dr. Eric Elder
School of Nuclear and Radiological Engineering / Medical Physics
Department of Radiation Oncology, Emory University School of Medicine

Dr. Sang Hyun Cho
School of Nuclear and Radiological Engineering / Medical Physics
Georgia Institute of Technology

Date Approved: July 2, 2007

TABLE OF CONTENTS

LIST OF TABLES

LIST OF FIGURES

SUMMARY

A Varian 2100C 18 MV photon beam has been modeled in this work using the MCNP5 Monte Carlo particle transport user code. The subsequent beam irradiation was also delivered to a water phantom and benchmarked against experimentally measured depth dose data. The model presented in this work establishes the foundation to which further beam characteristics tuning is required in order to realistically model the beam mentioned above. It has been determined in this work that the initial electron beam energy of this beam model is sufficiently close to the electron beam energy from the linear accelerator used to obtain the benchmark depth dose data.

Software was developed in this work that divides and configures the treatment head of a medical linear accelerator into several stages and generates the necessary MCNP input files that simulate the beam delivery based on user input. A 18 MV beam was created and collimated to a 4 cm by 4 cm square field size. This collimated beam was then delivered to a water phantom with 0.15 cm length cubic *F8 tally voxels spanning half of an in-plane profile from the central axis. Simulation times for the 3 stages of this configuration took approximately 7.3 hours, 8.4 hours, and 3.2 weeks for stages 1, 2, and 3 respectively.

Percentage depth dose values derived from average absorbed dose estimations along the central axis were found to be within ±2% at depths beyond the point of maximum dose deposition. Although the average values are accurate along the cax, the experimental error is undesirably high in some regions of the in-plane profile. The lateral absorbed dose estimations were higher toward the edges where the stereotypical ‘horns’ exist for higher energy megavoltage photon beams relative to the beam benchmark data.

CHAPTER 1

INTRODUCTION

The Monte Carlo method can be utilized to accurately simulate radiation transport and has been in practice for more than half of a century[1]. The Monte Carlo method provides the most accurate way of determining dosimetric estimations for radiation therapy treatment planning, especially in the presence of bone and/or lung heterogeneity. The Monte Carlo method is also useful to accurately determine absolute dose estimations in regions of highly varying dose depositions at the penumbra region and dose deposition in charged particle buildup / build-down regions. Widespread adoption of this method in radiation therapy physics is obstructed by the amount of computational time necessary to achieve statistically significant and reliable estimations.

Monte Carlo user codes currently exist that simulate radiation phenomena. The most popular Monte Carlo codes that have been used in Medical Physics are MCNP[2] and EGSnrc[3]. MCNP is a general purpose Monte Carlo, N-Particle user code maintained by the Diagnostics Applications Group at Los Alamos National Laboratory. MCNP can accommodate coupled neutron, photon, and electron transport. EGSnrc, (Electron Gamma Shower – National Research Council of Canada) is the continuation of a previous Monte Carlo photon and electron user code called EGS4. EGSnrc is also capable of simulating coupled electron and photon transport in general geometry.

Existing EGS-based user codes such as BEAMnrc[4] and DOSXYZnrc[5] could provide the same functionality as presented in this work. BEAMnrc simulates the clinical photon and electron beams for many models of medical linear accelerators from different vendors[6]. DOSXYZnrc is a simulation user code for calculating dose distributions in rectilinear three dimensional voxel phantoms[7]. Although the combination of the user codes BEAMnrc and DOSXYZnrc provide the same functionality as presented in this

work, that avenue would not easily allow for future additions that would combine form a robust Monte Carlo based, general purpose radiation therapy physics research tool.

A Varian 2100C model linear accelerator[£] has been modeled in this work using MCNP version 5.1.40. MCNP was selected as the basis of the software developed in this work for two reasons. The first reason stems from the simulation capabilities of the user code. MCNP uses a more sophisticated general source definition and is more flexible when specifying the simulation geometry. This will be useful in future additions that include brachytherapy and diagnostic imaging simulations where it is relatively difficult to simulate using EGSnrc. The second reason is derived from the desire to eventually create a general purpose radiation therapy physics research tool that is as adaptable as is feasibly achievable. It is the author's opinion that this research tool would be most quickly realized at this time using the MCNP code system.

Software designed as the basis for this research tool was developed in this work. It generates the necessary MCNP input files to model the Varian Clinac® 2100C 18 MV photon beam[£] in several stages and delivers the radiation to various phantoms. The first two stages are dedicated to generating and shaping the photon beam according to user specifications. The shaping components of the beam modeled within the first two stages consist of the primary collimator, vacuum window, flattening filter, and secondary collimators. The last stage is dedicated to simulating the water phantom or patient DICOM data and establishing the MCNP *F8 tally voxels in the particular type of phantom specified by the user. Post processing modules were also created that visualize and format the information within the MCNP output file such that third party visualization software can be used to analyze the results to a greater extent.

[£] Confidential Information, Varian Oncology Systems – Palo Alto, CA.

All computer simulations in this work were run in parallel on a computer cluster running the MPI build of MCNP version 5.1.40. The computer cluster consists of 20 computers with each PC having a ASUS A8N-SLI motherboard, AMD Athlon™ 64bit Dual Core Processor 4400+ (2.2GHz/processor), 2 Gbytes of physical memory, and a Gbit Ethernet NIC. The MPI build of MCNP5 was built with the free Intel Linux Fortran compiler version 9.0 in Linux Enterprise Edition 4.0. The implementation of MPI used was MPICH version 1.2.7.

CHAPTER 2

BACKGROUND AND THEORY

A linear accelerator (linac) that is used in the clinical setting generates, forms, and delivers beams of radiation typically composed of photons and electrons. Figure 2.1 shows the typical configuration of modern megavoltage linear accelerators used for radiation therapy. To begin producing radiation, a microwave source is fed into the klystron which produces another amplified microwave source. The amplified microwave power is then directed through the waveguide structure and circulator on its way to the accelerating structure. The circulator is necessary to prevent a backflow of microwave power that could both interfere with the klystron's ability to reliably amplify power and cause damage to the klystron[10]. After the circulator, the microwave power is then used to accelerate electrons emanating from the electron gun down the length of the accelerating structure. The electrons leave the accelerator structure and enter the treatment head in tightly formed bunches. Their trajectory is then deflected 270^{o} and are made incident onto the x-ray target for the case of photon beam generation.

The "treatment head" of the Varian 2100C linear accelerator was the linear accelerator section modeled in this work. The individual components of a typical treatment head of a medical linear accelerator are given in Figure 2.1. Shown in the expanded view of the treatment head are most of the modern components which are used to produce and shape the photon beam for therapeutic use. The x-ray target, primary collimator (now shown), flattening filter, and secondary collimators (labeled as *collimators* in Figure 2.4) were modeled in this work. These components used together are sufficient to produce a realistic photon beam. Other components in the treatment head are important to model as they provide additional sources of radiation that contribute to the deposition of more energy per starting electron or Monitor Unit (MU).

This contamination (mostly electron contamination) has recently been identified and quantified by Chibani and Ma[11].

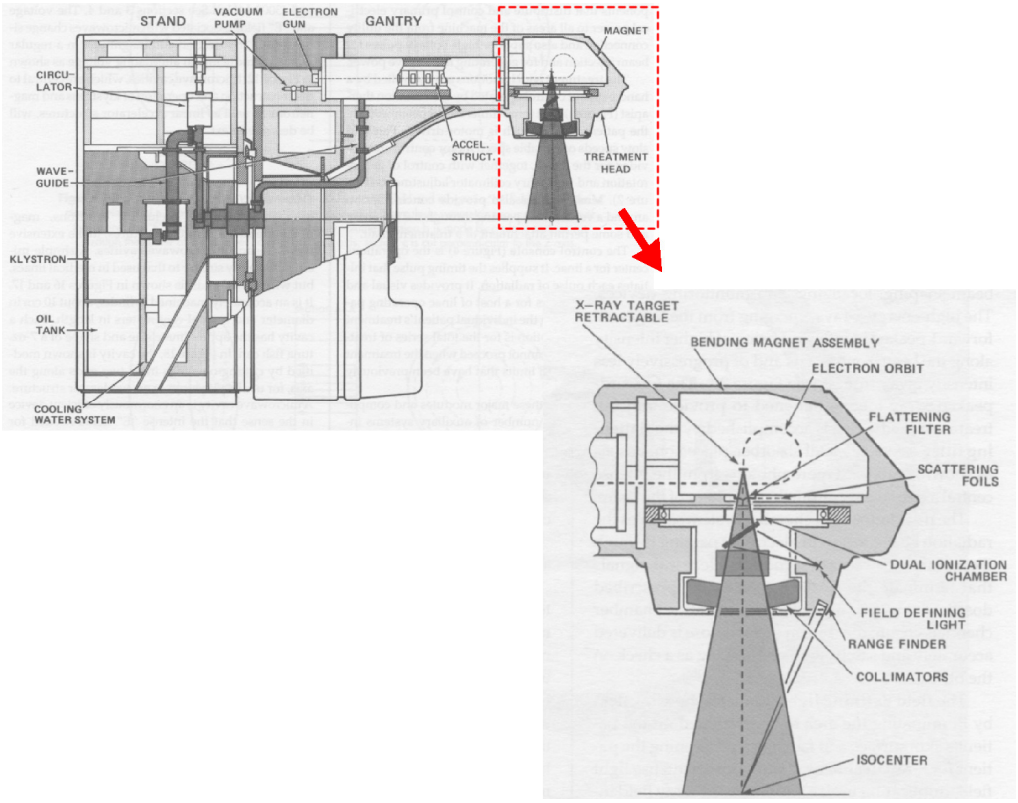

Figure 2.1: Typical medical linear accelerator used in radiation therapy treatment.[10]

CHAPTER 3

PROBLEM APPROACH

Stages in the modeling process were designed to increase the reusability of the simulations and thus lessen occupied computer cluster time. The components from the Varian 2100C 18 MV photon beam that were modeled in this work, along with the simulation stage in which they belong are illustrated in Figure 3.1. During the simulation, Phase Space data Files (PSFs) are used to record particles of interest that cross specified surfaces. Stages 1 and 2 collect radiation particle type, energy, weight, position, and direction from the simulation and stages 2 and 3 utilize the previous stage's PSF as a source of radiation. All radiation in the simulation is derived from an initial source of unidirectional, 18 MeV electrons incident upon a point on the electron target that lies on the central axis (cax).

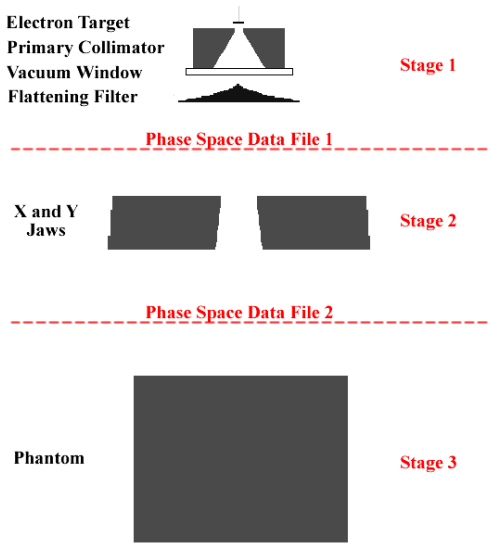

Figure 3.1: Simulated components of the treatment head along with respective simulation stage.[℘]

[℘] Original image obtained from Monte Carlo Refresher Course – AAPM 2002 Siebers – Virginia Commonwealth University.

The software developed here is designed to generate multiple configurations within each stage of this Varian 2100C linac simulation. Although the 18 MV beam was the only beam simulated and benchmarked against experimental data to date, stage 1 can either be a 6 MV photon beam or an 18 MV photon beam. The generation of the stage 2 input file requires that the user specify field size and collimator rotation. The maximum field size permitted is a 40 cm^2 square field size. Stage 3 can simulate the dose delivery to either a water phantom or a DICOM based dataset.

Stage 3 input file generation is slightly more involved than what is required to generate stage 1 and 2 input files. The software currently defaults to the creation of a 30 cm x 30 cm x 50 cm-deep water phantom that relies on user input to specify *F8 tally voxel start location, voxel dimensions, and length of tally region. Earlier versions of MCNP have been observed to slow down dramatically when simulating large numbers of cells[12] and measures were taken to circumvent this issue in cases where the user must simulate a large number of cells. There is a capability of producing multiple stage 3 input files that allow for volume distributions to be obtained, unfortunately at the expense of multiple simulations. Each simulation could then be put together to obtain dose volume information assuming enough particles were simulated and well-converged estimates of absorbed dose in each voxel were calculated for each individual simulation.

Figure 3.2 shows an isometric drawing of a 4 cm x 4 cm field size photon beam with no secondary collimator rotation irradiating the water phantom. Cubic tally voxels 0.15 cm on each side have been specified to cover half of an in-plane profile extending 4 cm in the x-direction from central axis (cax) and 40 cm deep from the surface. This was an experimental arrangement that was simulated and benchmarked against identical experimental conditions with beam data collected from The Emory Clinic linac station 3

(TEC3)[ξ]. The accuracy of the simulation will be compared to in-plane beam dose information measured with a farmer ionization chamber in a water phantom.

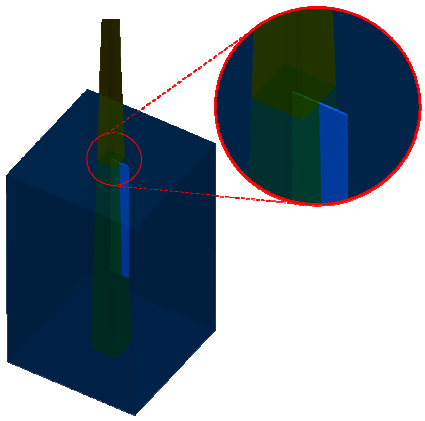

Figure 3.2: Isometric drawing of 4 cm x 4 cm field size photon beam irradiating a water phantom. Possible scenario of tally voxels are colored in light blue.

The other stage 3 option simulates radiation transport through orthogonal hexahedra, three dimensional rectilinear voxel arrangement derived from a DICOM volume dataset. The Insight Toolkit (ITK) was used to interface DICOM data and perform other image processing procedures to format the information so that it would be more conveniently represented in the MCNP stage 3 input file. This software module relies on two input files that the user must tailor to his/her specific requirements.

The first input configuration file for the DICOM based stage 3 input file contains the specifications on how MCNP material will be interpreted from Hounsfield Unit (HU) values in the DICOM dataset. An approximation of the HU units relating to MCNP material assignment is illustrated in Figure 3.3. An example configuration is given in Figure 3.4 demonstrating the appropriate syntax. One must specify the HU range that can

---

[ξ] Emory Winship Cancer Institute in Atlanta, GA

be applied to generate the input file. The material specifications must be in order of increasing HU units while also containing a MCNP material 'keyword' to match that which is presently hard-coded into the software. Air, Water, and ICRU Compact Bone are the 3 materials available at this time. The integer following the material 'keyword' is the material card number formatted within the MCNP input file. The unusually high HU for compact bone is the upper-bounded value in a tested DICOM dataset which contains a metallic buckle on a restraining belt caught within the imaging domain, (see Figure 3.6).

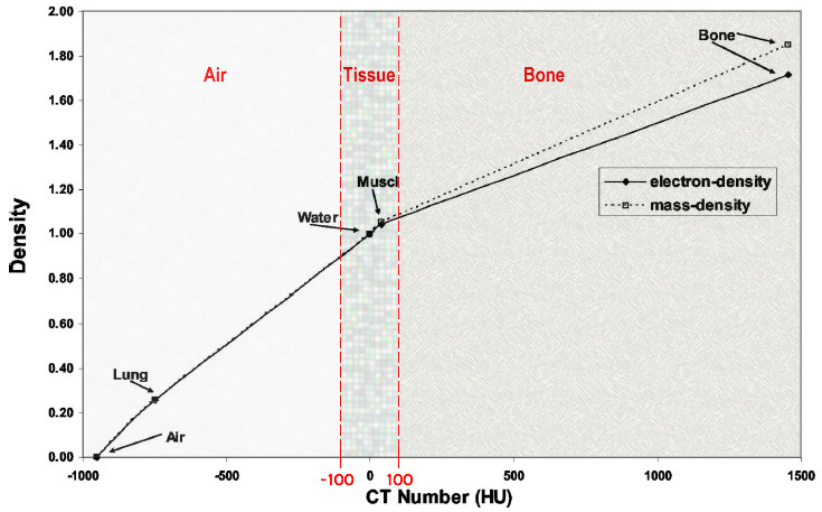

Figure 3.3: Approximate material range specification for hounsfield unit to MCNP material conversion.[13]

```
Materials must be in order of increasing CT values

<Material>
air
1
-1000 -100
m1 ..air
</Material>

<Material>
soft tissue
2
-100 100
m3 ..tissue
</Material>

<Material>
bone
3
100 13655
m4 ..bone
</Material>
```

Figure 3.4: Input file used for hounsfield unit to MCNP material conversion. File referred to as mcnphumateriallib for use in the second input file for stage 3 DICOM.

The second input configuration file for the DICOM based stage 3 input file contains most of the conditioning parameters that format the DICOM dataset for use in MCNP. Figure 3.5 shows the parameters that the software requires to successfully generate the DICOM-based stage 3 input file. All parameters except for the isocenter specification are used in generating the DICOM-based stage 3 input file. The isocenter of the phantom is hard-coded to be the midpoint of the most anterior surface of the cropped image information. Efforts to date have been to demonstrate functionality of this implementation of stage 3. An isocenter 'hook' was included for future improvements that include the addition of a graphical user interface and visualization capabilities to further aid the researcher in more accurately establishing the simulation environment.

```
dicom original directory
C:\jared\src\Phantom\alteredRbH1_20k

dicom cropped directory
C:\jared\research\MS_Thesis\code\CroppedDicom

mcnp hu material library
C:\jared\research\MS_Thesis\code\MS_Thesis\mcnphumateriallib

isocenter
1.123456789e9 2.123456789e9 3.123456789e9

crop origin
181 144 276

crop dimensions
148 184 74

generate homogenized image
yes

homogenize blocks
74 92 74
```

Figure 3.5: Input file containing file locations and image processing directions for the stage 3 DICOM based MCNP input file.

The second input configuration file has the capability of condensing the raw image resolution to a much coarser resolution. The parameter '*generate homogenized image*' set to '*no*' will generate an MCNP material image of the cropped image region at the original resolution. Setting the same parameter to '*yes*' will read the number of

voxels specified with the '*homogenize blocks*' parameter and average the appropriate voxels values that constitute the new voxel region. The average HU value for each new coarser voxel will then be converted to its equivalent MCNP material using the HU ranges in the first input configuration file, (Figure 3.4). It should be noted that it is the researcher's responsibility at this point to find third party visualization software to help in determining voxel cropping dimensions. The image processing and analysis software, ImageJ[ς] was found to be very useful for the purposes of determining the cropping region.

The testing of the DICOM-based stage 3 MCNP input file generating module will be used on a DICOM dataset of an ART male phantom model. The image dataset that is visualized with VolView 2.0 shows the phantom dataset below in Figure 3.6. A cropped image region around the head and slightly down the neck will be used to reduce the number of voxels produced in the MCNP input file as is shown below the VolView software.

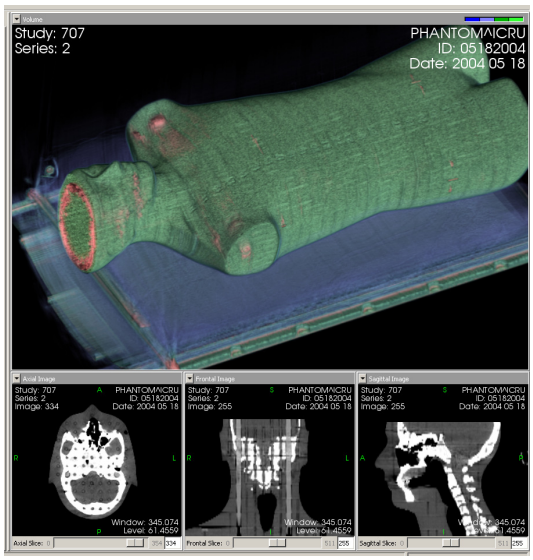

Figure 3.6: ART Anthropomorphic Male Phantom viewed with VolView 2.0[Ψ].

[ς] ImageJ – Image Processing and Analysis Software developed by Wayne Rasband at NIH
[Ψ] VolView Software, Kitware Inc., http://www.kitware.com/products/volview.html

CHAPTER 4

DATA AND RESULTS

The software developed in this work was used to create the necessary input files that are required to simulate the Varian 2100C 18 MV photon beam in MCNP. A 4 cm x 4 cm square field size was created for stage 2 of the simulation. Additionally, a stage 3 water phantom was used to gather dosimetric information that characterizes the beam and determines its adequacy in representing a realistic photon beam compared to experimental data obtained from The Emory Clinic linac station 3 (TEC3). Shown in Figure 3.2, half of an in-plane profile was defined with 0.15 cm length cubic voxels and the *F8 tally was used to record the absorbed dose deposition for the simulation.

The Insight Toolkit (ITK) and the Visualization Toolkit (VTK) were used to visualize the results obtained from the MCNP output file at the end of stage 3 shown in Figure 4.1. A voxel size of 0.15 cm on each side was used in this simulation extending approximately 4 cm on the x-axis from cax and approximately 40 cm deep into the phantom. Half of the in-plane profile was collected and is assumed be symmetrical about the central axis although this is rarely ever the case in the clinical setting. The dosimetric information was mirrored appropriately to show how the beam absorbed dose distribution would appear for the whole in-plane profile. The data is normalized to the point of maximum dose within the in-plane profile and in this case is located within the stereotypical ‘horns’ that exist off-axis in higher energy megavoltage photon beams. The grey area indicates regions that were tallied in the simulation but were less than the minimum isodose visualization limit. In this instance, the grey area indicates a region having an isodose that is calculated to be less than 10%.

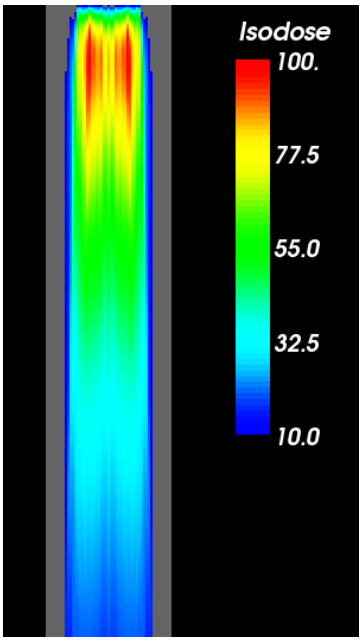

Figure 4.1: Visualization of 4 cm^2 field size, in-plane profile of isodose values normalized to d_{max} in the entire profile. Half of an in-plane profile was measured and the data was mirrored to further demonstrate the beam characteristics.

Figures 4.2 through 4.9 shown in the following pages give the typical comparisons of this simulation with experimentally measured beam data obtained from TEC3[¥]. Unlike Figure 4.1, these figures will all be normalized to the measured point of maximum dose along the cax. The '*interp2*' interpolating function with the '*cubic*' implementation in MATLAB 7.0.1 was used to calculate the simulated values in locations where the centroid of the simulated voxels do not exist where TEC3 data points were collected. Figures 4.3 through 4.9 will consist of two figures each. The first figure (*a*) gives the absorbed dose comparison to that of TEC3. The second figure (b) shows the percent error of the difference of simulated average value from that recorded with TEC3.

[¥] The Emory Clinic linac station 3, Winship Cancer Institute, Atlanta GA.

All dashed lines in (*a*) represent the error bounds of the solid line plot having the same color.

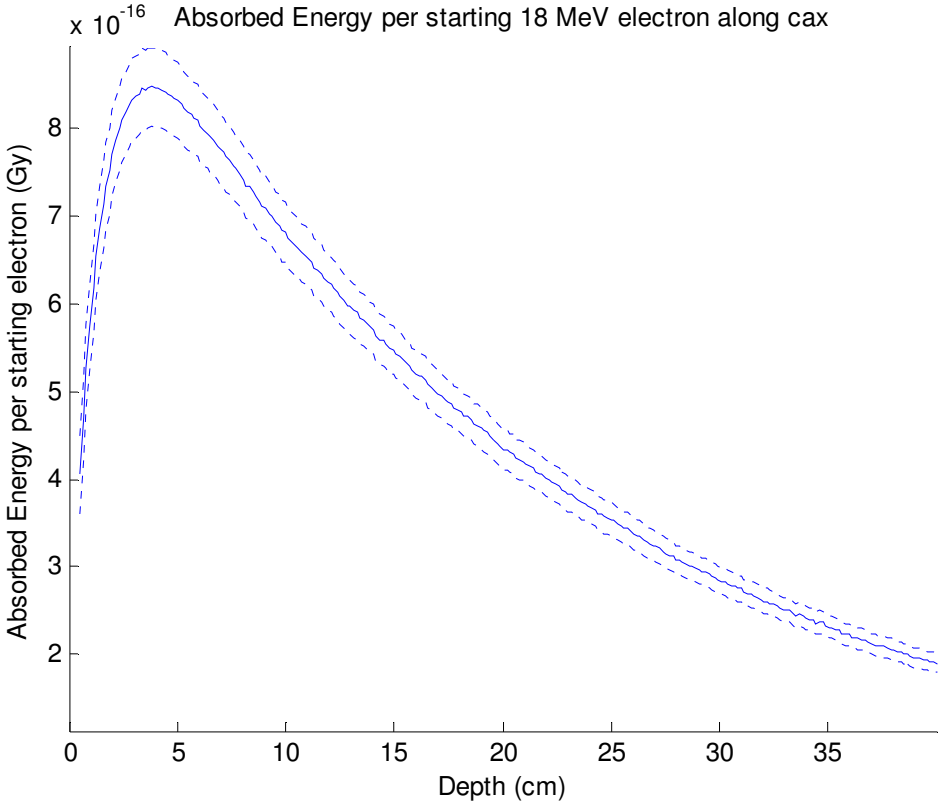

Figure 4.2: Simulated absorbed dose in Gy along cax. Error in simulation given by included region within dashed lines.

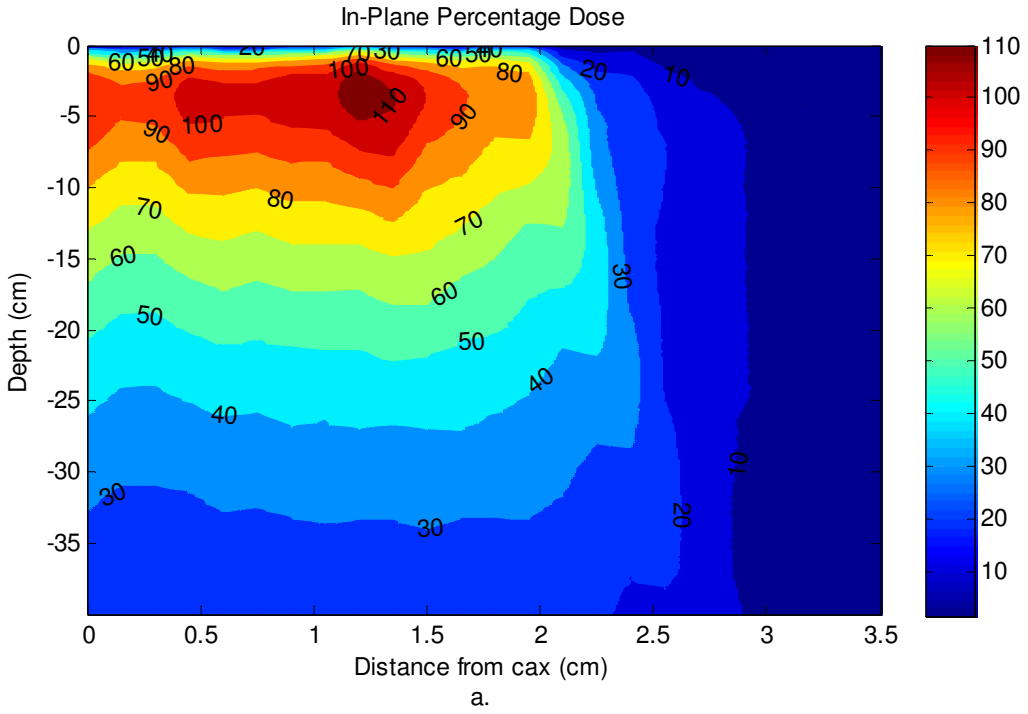

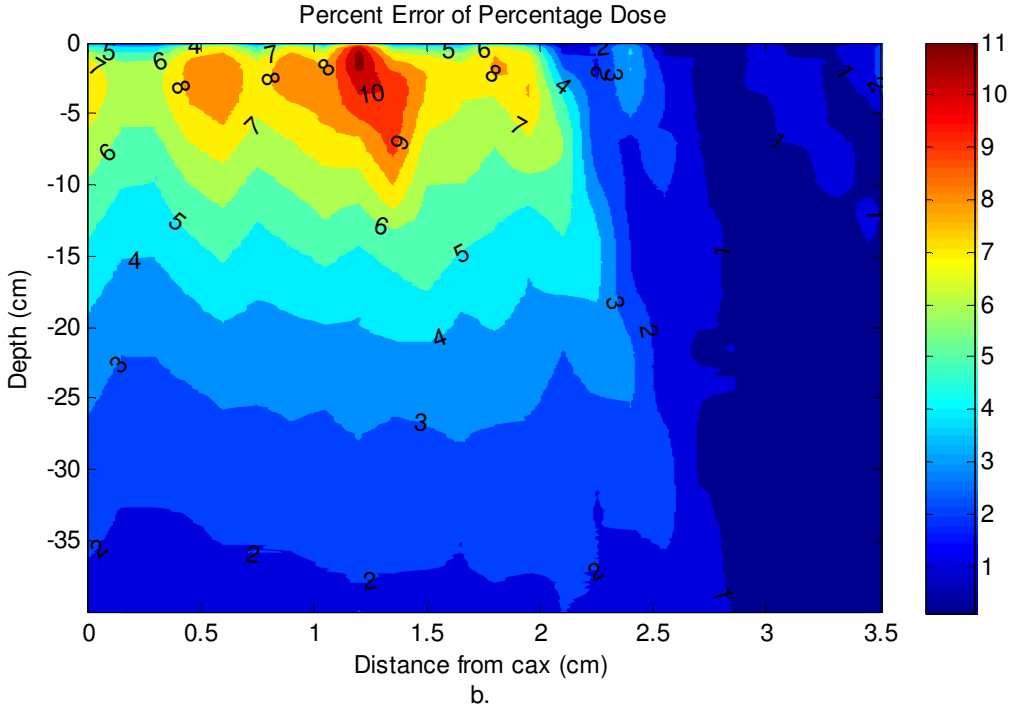

Figures 4.3: Contour plots of percentage isodose values normalized to point of d_{max} measured along the cax. (a) shows the isodose cont\our plot and (b) shows the percentage error of the simulated percentage depth dose.

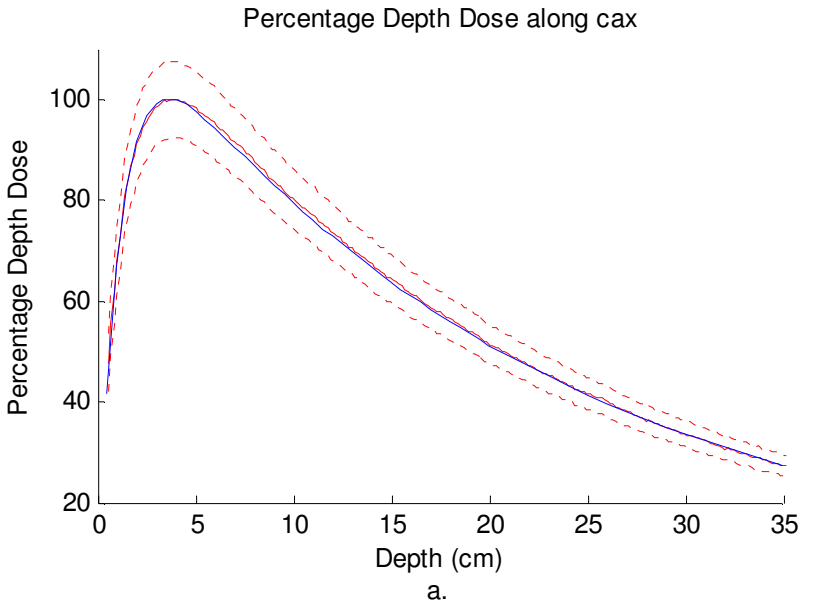

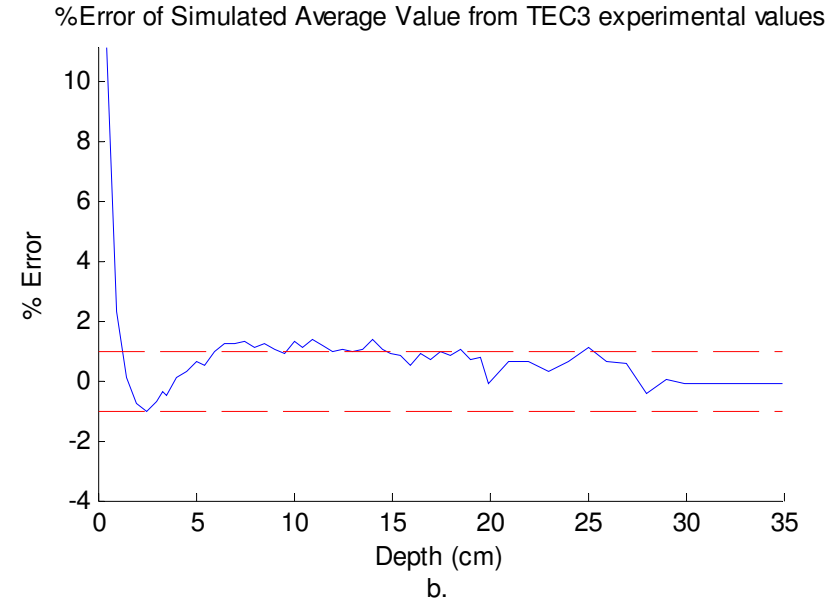

Figures 4.4: Percentage depth dose along cax. Values normalized to point of d_{max} measured along the cax. (a) shows PDD with experimental error and (b) shows the percentage error of the simulated average value from TEC3. Dashed lines in (b) indicate the ±1% error bounds.

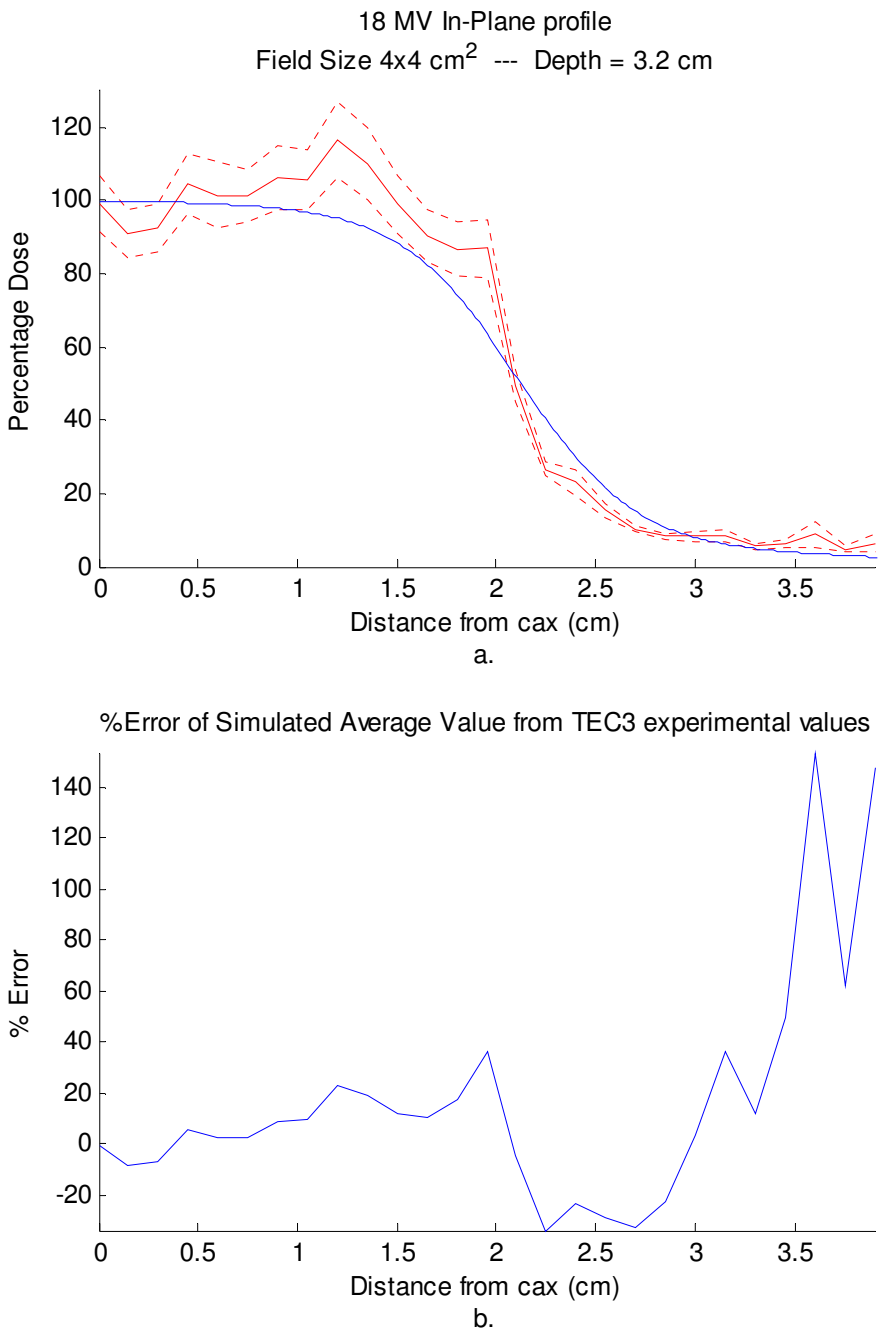

Figures 4.5: Percentage dose along along 3.2 cm in-plane profile. Values normalized to point of d_{max} measured along the cax. (a) shows percentage dose with experimental error and (b) shows the percentage error of the simulated average value from TEC3.

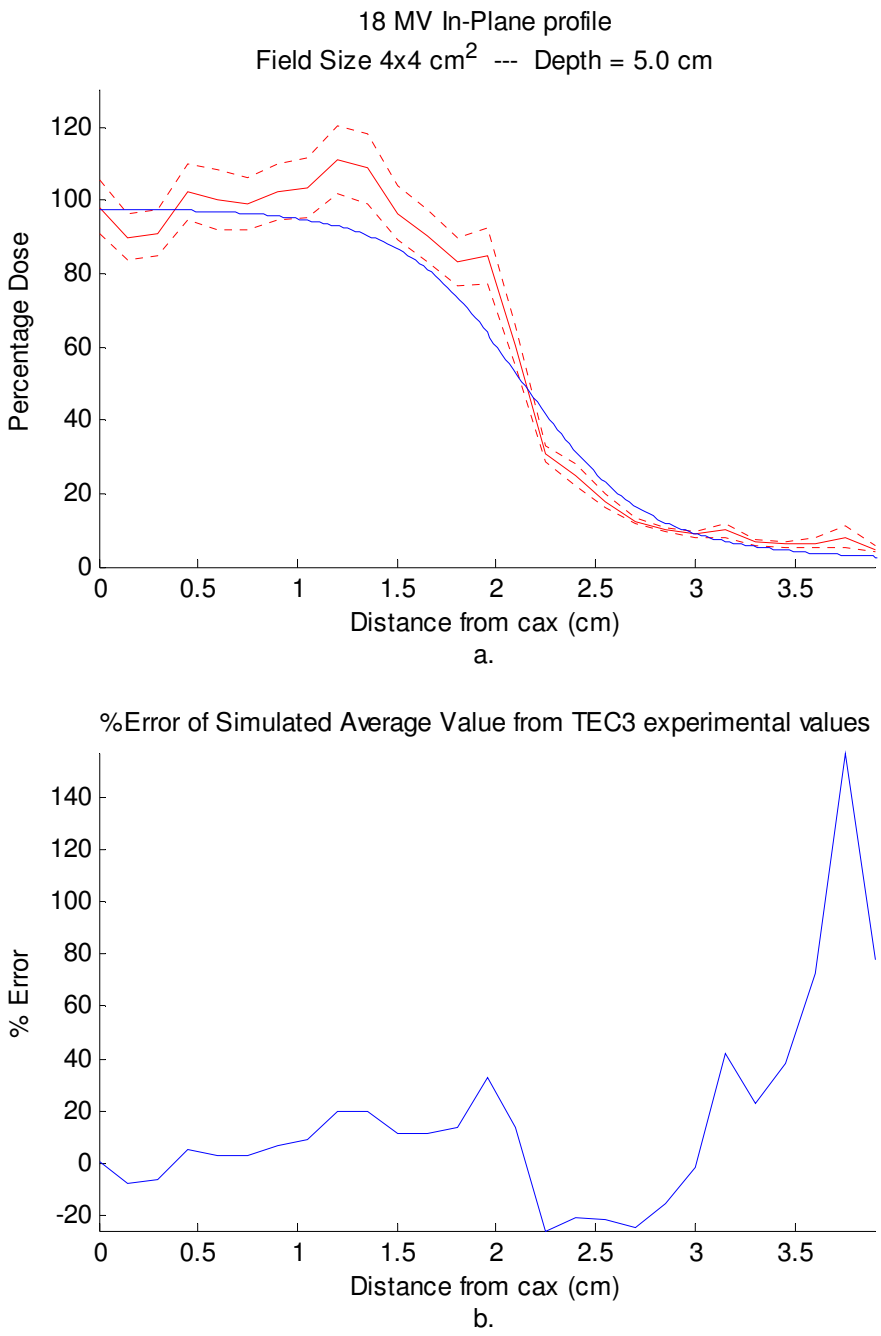

Figures 4.6: Percentage dose along along 5.0 cm in-plane profile. Values normalized to point of d_{max} measured along the cax. (a) shows percentage dose with experimental error and (b) shows the percentage error of the simulated average value from TEC3.

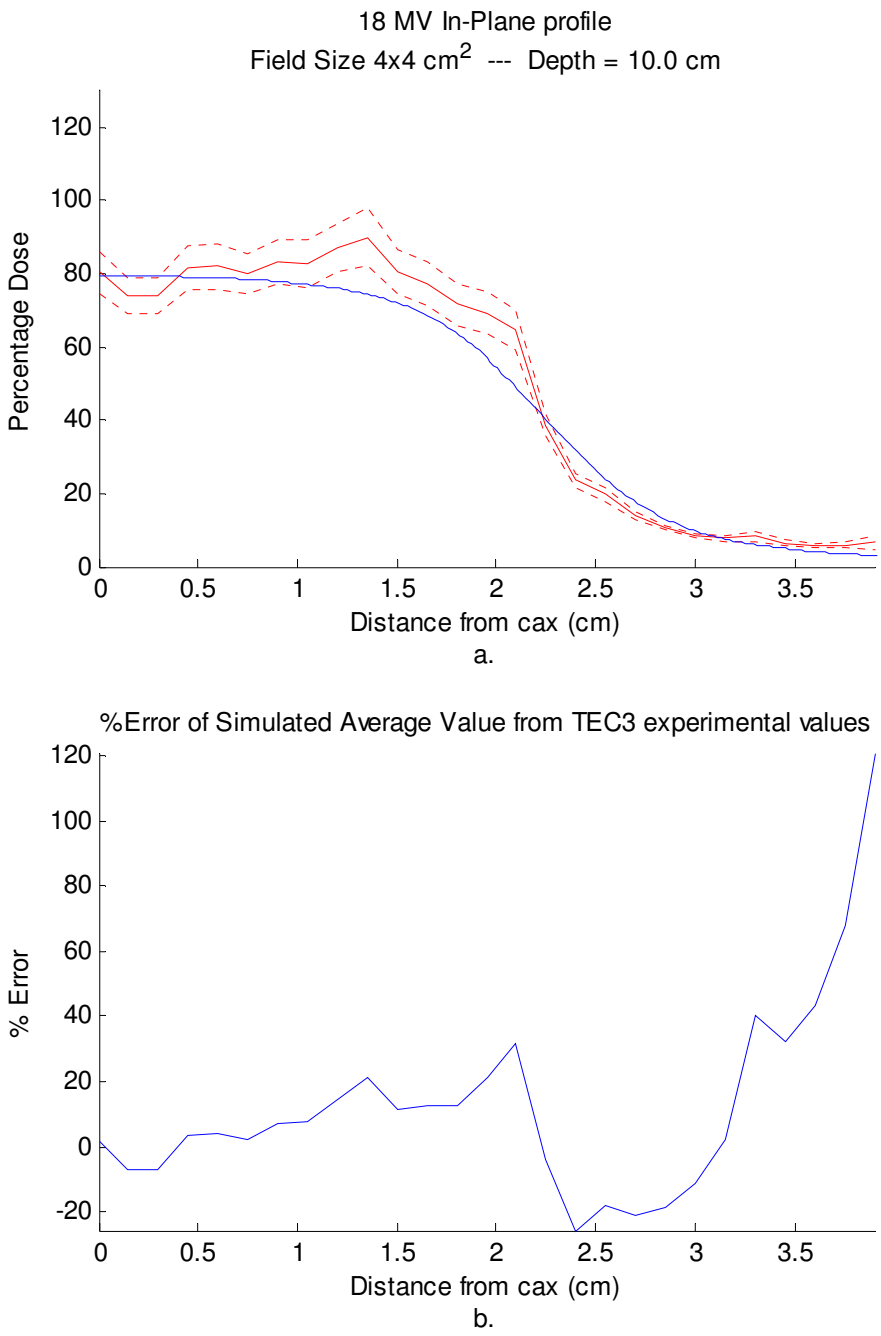

Figures 4.7: Percentage dose along along 10.0 cm in-plane profile. Values normalized to point of d_{max} measured along the cax. (a) shows percentage dose with experimental error and (b) shows the percentage error of the simulated average value from TEC3.

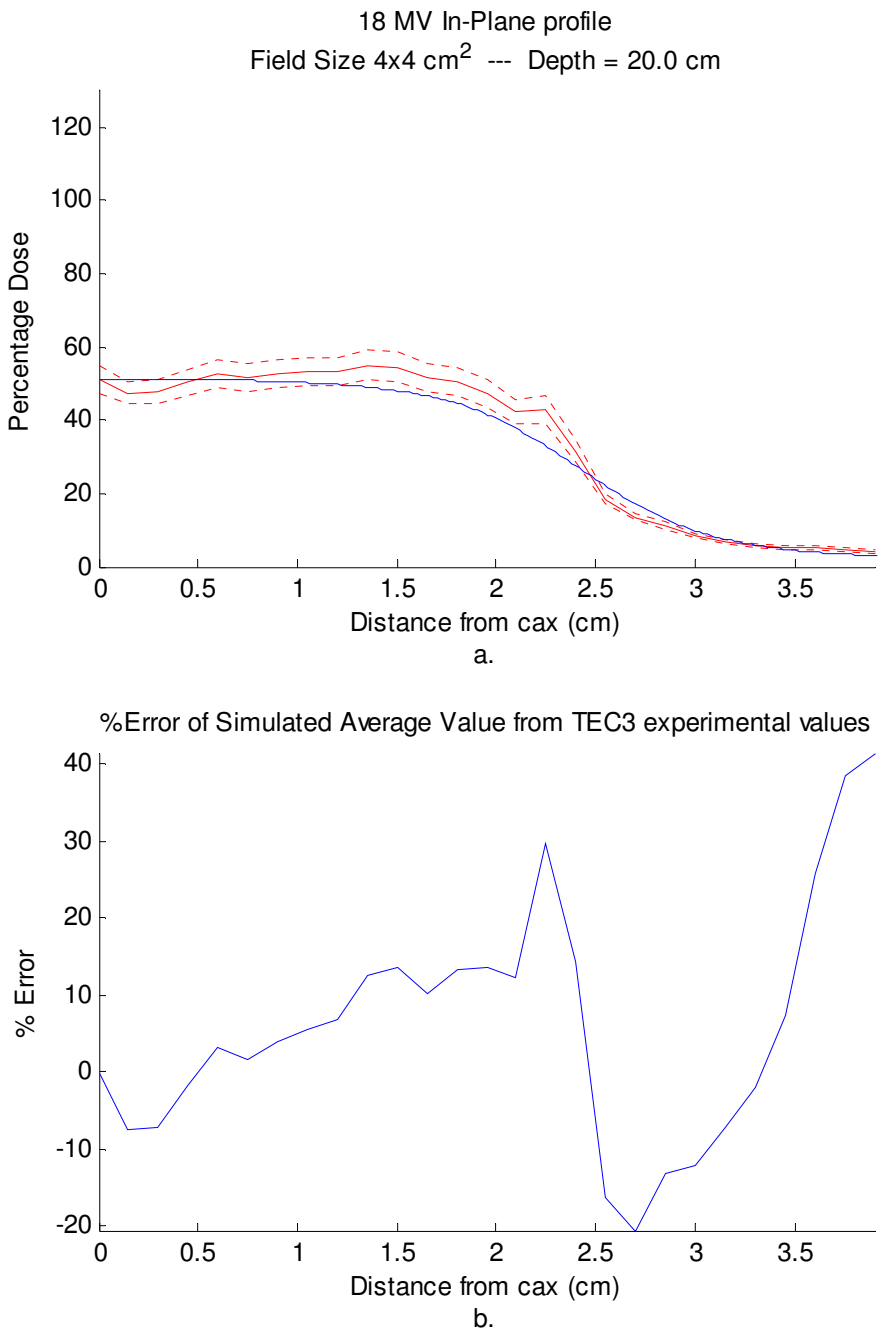

Figures 4.8: Percentage dose along along 20.0 cm in-plane profile. Values normalized to point of d_{max} measured along the cax. (a) shows percentage dose with experimental error and (b) shows the percentage error of the simulated average value from TEC3.

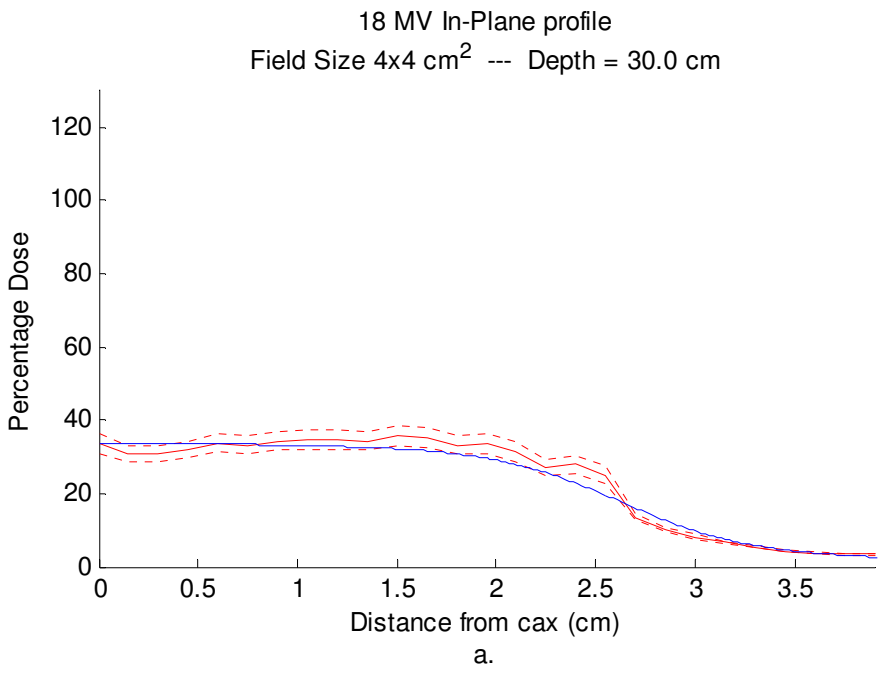

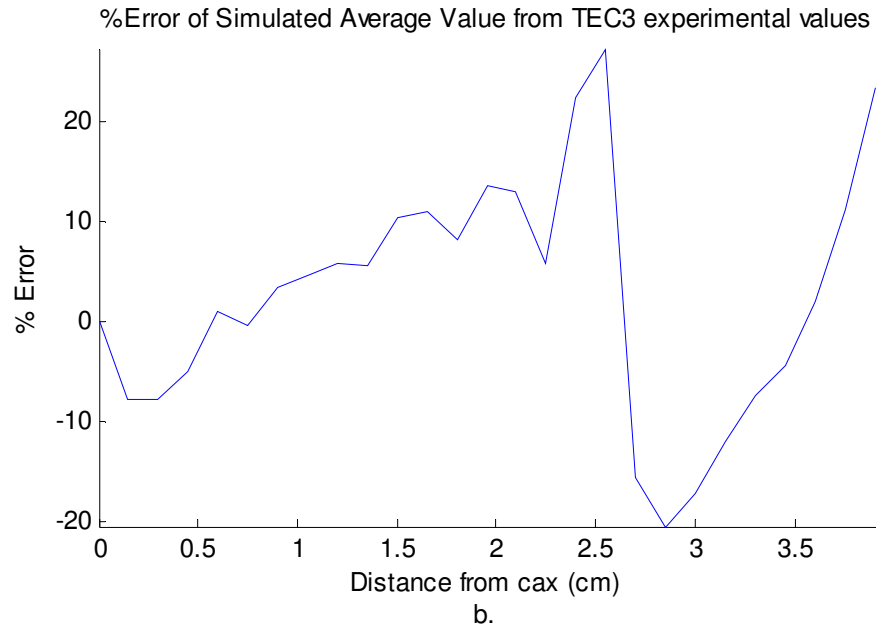

Figures 4.9: Percentage dose along along 30.0 cm in-plane profile. Values normalized to point of d_{max} measured along the cax. (a) shows percentage dose with experimental error and (b) shows the percentage error of the simulated average value from TEC3.

The DICOM-based stage 3 input file was generated and tested but there was unfortunately not enough time to run the MCNP simulation. The original resolution of the DICOM dataset used is listed in Table 4.1 (*a*) and visualized in Figure 3.6. Cropping a small head and neck region and homogenizing that dataset to produce a coarser representation of the original phantom still generated a MCNP input file containing more than 10^4 cells. It had been attempted to run the simulation in MCNP but progress slowed down seemingly to a stop and the simulation was discontinued from that point.

Figures 4.10 and 4.11 give digital image representations of the formatted DICOM datasets in order to demonstrate the voxel homogenization and MCNP material designation used when generating the DICOM-based stage 3 input file. The range of the HU within the datasets was rescaled to an *unsigned char* data value of 0 to 255. Table 4.1 gives the resolutions of image datasets (*a*) through (*f*). The red lines in Figures 4.10 show where the axial slice was taken from the sagittal slice to be displayed in Figures 4.11. Each individual letter in Table 4.1 and Figures 4.10 and 4.11 belong to the same dataset. Data sets (*d*) through (*f*) are the MCNP material representations of the cropped dataset.

Various resolutions were homogenized here to show how well that the new image datasets represented the original dataset before and after the transformation. Datasets (*a*) and (*d*) represents the cropped DICOM region at the original resolution. Datasets (*b*) and (*e*) condense the original AP/PA and L/R directions to half of the original resolution. Datasets (*c*) and (*f*) condense the original AP/PA and L/R direction to a quarter of the original resolution and the axial direction to half of the original axial resolution.

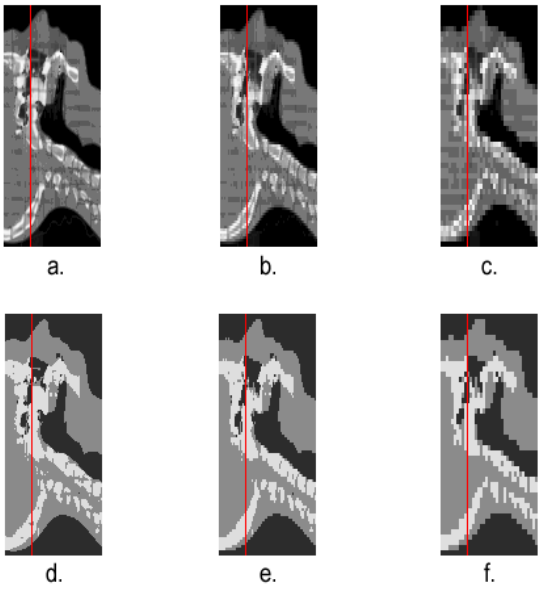

Figures 4.10: A sagittal slice of the cropped image datasets derived from the original DICOM dataset. Red line indicates the axial slice taken to be displayed in Figures 4.11. Resolutions of datasets are given in Table 4.1

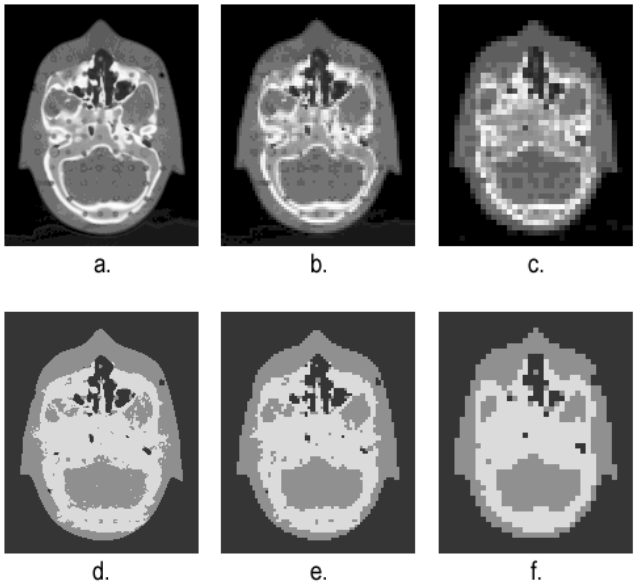

Figures 4.11: Axial slices of the cropped image datasets derived from the original DICOM dataset. Resolutions are given in Table 4.1.

Table 4.1: Figures 4.10 and 4.11 Spatial resolution after homogenization and MCNP material designation.

	All Spatial Resolutions (mm)					
	a.	b.	c.	d.	e.	f.
Anterior / Posterior	1.26953	2.53906	5.07812	1.26953	2.53906	5.07812
Left / Right	1.26953	2.53906	5.07812	1.26953	2.53906	5.07812
Inferior / Superior	2.5	2.5	5.0	2.5	2.5	5.0

CHAPTER 5

DISCUSION

The most prevailing observation of the dosimetric information obtained from these simulations is the high experimental uncertainty. It would have been desirable to achieve absorbed dose deposition accuracy to within 2-3% everywhere in the phantom. Although achieving this accuracy would have been possible from strictly a Monte Carlo method point of view, it would likely push the limits of how well this simulation represented the actual operation of this 18 MV photon beam and further measures must be taken to tune this 18 MV beam.

The common remedies to eliminate poor statistics in Monte Carlo radiation simulations are to run more particles, introduce variance reduction techniques, and/or alter the tally geometry in order make tally convergence more favorable. Variance reduction techniques were kept to a minimum for reasons to be discussed later. It would have been possible to change the tally geometry within the water phantom from 0.15 cm voxels to concentric cylinders stacked upon one another[14]. This would utilize more interaction events that contribute to the convergence within the final output values but it would have defeated the purpose of attempting to simulate a Monte Carlo transport beam delivery with practical types of geometry. The remaining option was to run more particles.

The issue with running more particles is related to the limitation of the PSF size that can be used with the standard source MPI build of MCNP5. After running the stage 1 input file a few times varying the initial number of incident electrons, it appears that a 600 Mb PSF size is approximately the largest file size allowed without altering the MCNP source code. PSFs larger than this that are used with the MPI build of MCNP5 on our computer cluster would throw MPI library related errors in a seemingly infinite loop. Accepting this limitation for the time being as an inevitability of using MCNP, it

introduced a bottleneck effect for collecting beam information in the first PSF. The outcome of allowing this stage 1 limitation is the questionable representation of source photon distributions (and 18 MV beam characteristics) contained within the second PSF that is sampled in the stage 3 simulation.

The MCNP surface source read and write cards (SSR and SSW, respectively) were used for creating and reading the PSFs generated during these simulations. The number of particles (NPS) card determines how the source particles are sampled when reading PSFs in MCNP. The proper sampling of particles is maintained by MCNP depending whether the user specifies more or less particles relative to the initial source particles[15] in the stage 1 simulation. The 600 Mb file size limitation in stage 1 allowed 3E6 initial 18 MeV electrons to produce 6.3E6 photons with a slight bremsstrahlung biasing applied (BBREM card) for the first PSF. The number of available photons was reduced to approximately 9E4 after the 4 cm x 4 cm square field size beam shaping in stage 2. These 9E4 photons were reused approximately 5E5 times to produce the results presented in the Data and Results section of this document. The stage 3 simulation running in parallel took approximately 3.2 weeks to complete.

Additional variance reduction techniques could have been used during these simulations to reduce both the total computation time and stage 3 simulation error but were instead kept to an absolute minimum. Verhaegen and Seuntjens[16] gathered a series of procedures that are valuable when tuning the primary electron beam characteristics of a simulated linac model. The first procedure that is suggested to tune the linac model is to zero in on the initial electron energy and subsequently compare depth dose along cax with experimental data measured from the equivalent linac model. It was also suggested that using a small secondary collimator field size would help reduce the amount of in-scatter that could slightly disrupt the measurement. A match in initial electron energy was said to occur when local depth dose values beyond the point of d_{max} is less than 2%. Normalization of absorbed dose information to obtain percentage depth dose (PDD)

information was also suggested to be normalized to a depth of 10 cm since that point will contain a lesser amount of statistical noise that propagates throughout all data points.

Default photon and electron transport cutoff parameters in MCNP were used in this stage 3 simulation to achieve a more accurate dose deposition considering the unusually small 0.15 cm cubic tally voxels in the water phantom. It would have been wise to also increase the number of electron substeps *m* used in each electron energy transport step[15] but instead was kept at the default value of 3 to complete the simulation in a shorter amount of time. The average values of cax depth dose obtained from the simulation (Figure 4.4a) are within 2% of TEC3 experimental values (Figure 4.4b). The error associated with the simulation is undesirably high in some regions of the in-plane profile.

The first fine tuning procedure originally suggested by Lin *et. al.*[17] does not require comparing values in the buildup region approaching the point of d_{max}. Until recently, Monte Carlo simulations of 18 MV photon beams have inaccurately estimated the absorbed dose leading up to d_{max}. Chibani and Ma[11] have very recently published work that suggests possible sources of this discrepancy. Additionally, they identified specific components of the linac head and quantified various contributions of photon and electron contamination that are missing in preceding 18 MV photon beam models. The stage 1 and 2 simulations in this work were optimized to record photons with energies above 300 keV in the PSFs while electrons were excluded from the PSFs recordings. Considering the lack of source contaminating radiation accounted for in this work, measurements at shallow depths still produced higher average absorbed doses than what was measured with TEC3.

The tuning of the linac beam characteristics beyond the first step that is given by Verhaegen and Seuntjens[16] was not attempted in this work due to time constraints. Figures 4.5 through 4.9 are given to show the lateral profiles that are generated from an initial electron monodirectional pencil beam distribution. It has been shown in many

instances that lateral dose depositions are influenced by linac component density variations and the radial spread of the electron position incident on the electron target rather than the small variations in incident electron energy[18] [19] [20]. Lin *et. al.*[20] found that smaller electron spot sizes incident on the electron target led generally to larger relative doses towards the edge of the field. The experimental data obtained in this work (Figures 4.4 through 4.9) are consistent with their observations.

The capability of delivering this 18 MV photon beam to orthogonal hexahedra, three dimensional rectilinear DICOM based voxels was completed but not tested in this work. Figures 4.10 and 4.11 show the digital image representations of the voxel homogenization/reduction and MCNP material designation. An effort was placed on creating a MCNP DICOM based stage 3 input file that contained a minimal number of cells that would still accurately approximate the original phantom image dataset. The coarsest voxel resolution was taken to approximately 0.5 cm on each voxel side and still introduced over 10^4 cells in the generated MCNP input file. Further voxel reduction beyond this resolution would speed up the computational time in MCNP but the dose deposition accuracy obtained renders it worthless for nearly all clinical purposes. MCNP source code modifications to optimize the memory management of large voxel number datasets could resolve this issue[21]. Additionally, examples using MCNP lattice structures for medical physics related simulations have been used to speed up computational time[14].

CHAPTER 6

CONCLUSION

The first steps in modeling the Varian 2100C linac 18 MV photon beam have been accomplished in this work. Further turning of the electron radial spread incident on the electron target in the stage 1 input file should be modified so that the photon beam more accurately simulates the in-plane dosimetric characteristics as is measured with TEC3. The initial framework of the software developed and linear accelerator components modeled serve as a solid foundation where additional beam components can be included and auxiliary uses of the software may be derived.

The restriction on the stage 1 PSF mentioned in the previous section introduced a questionable representation in the photon beam which in turn propagated throughout the entire simulation. It would be preferable to simulate enough stage 1 18 MeV electrons such that the second PSF contained a surplus of available photons to eliminate the need for repeating photons in the stage 3 delivery. It was assumed for the purposes of this work that the 9E4 photons collected in the second PSF adequately represented the 18 MV beam fluence characteristics. Results shown in Figure 4.4a may suggest an adequate PSF representation of the beam characteristics but further investigations should be performed to determine if this is actually true.

The percentage depth dose along cax was very close to that measured with TEC3 experiments. The depth dose average values simulated were within ±2% of the average values measured with TEC3. This is disregarding the deviation that exists before the depth of maximum dose deposition. This is a reliable indication that the initial electron energy modeled in stage 1 of this simulation is sufficiently close to the incident electron

energy of TEC3[17][18]. Following the suggestions offered by Verhaegen and Seuntjens[16], future improvements to this beam model may continue by adjusting the radial spread of electrons incident on the electron target. This should reduce the 'horns' that appear towards the edge of the in-plane profile (Figures 4.5 through 4.9) and influence the penumbra shape to match more closely to the penumbra shape of TEC3[17].

The MCNP simulation error could have been reduced to an acceptable level by modifying the simulation environment. Future improvements should require this in order to reduce the experimental error below 3% in all of the simulated values. Larger tally voxels would be an effective way to reduce the simulation error observed in this work and assist in converging the experimental values more rapidly. Another major improvement would be to apply more liberal variance reduction parameters. Higher variance reduction parameters for the transport cut-off energies of photons and electrons would significantly reduce the required computational time. The last suggestion to reduce experimental error in the percentage depth dose is mathematically based. When normalizing the percentage depth dose data, normalize to a point where the uncertainty is less such that the propagated error is reduced. This is commonly taken at a depth of 10 cm for high energy megavoltage photon beams[16].

The DICOM based stage 3 module should be restructured in future improvements to the software. The module should express the DICOM information with the MCNP lattice structure instead of a 1:1 ratio of MCNP cells to voxels with the current implementation. This should utilize several speed-up algorithms that have been designed in MCNP to streamline the types of computational requirements that are found in the typical medical physics radiation therapy beam delivery simulations.

The software developed in this work has the potential of becoming a valuable dosimetric analysis tool for Medical Physics purposes. It will be necessary to modify the MCNP source code in an effort to eliminate the MPI related memory restriction on the first PSF. This will allow a very realistic PSF to be produced for the final beam delivery stage of this software. It would also be very useful to apply the same MCNP modifications implemented by Wang *et. al.*[21] such that unnecessary computation and simulation output information are minimized.

REFERENCES

[1] Metropolis, N., *The Beginning of the Monte Carlo Method*, Los Alamos Science, Special Issue, 1987.

[2] Goorley, T., Bull, J., Brown F., *et. al*., MCNP Monte Carlo Team, X-5, *MCNP5.1.40 Code System*, Los Alamos National Laboratory, Oct. 3, 2005.

[3] Ionizing Radiation Standards Group – National Research Council of Canada, *EGSnrc V4-2-2 Code System*, National Research Council of Canada, Sept. 21, 2006.

[4] Rogers, D. W. O., Walters, B., Kawrakow, I., *BEAMnrc Cody System,* National Research Council of Canada, 2006.

[5] Walters, B., Kawrakow, I., Rogers, *D. W. O., DOSXYZnrc Code System*, National Research Council of Canada, 2006.

[6] Ionizing Radiation Standards Group, "*BEAMnrc Homepage: http:/www.irs.inms.nrc.ca/BEAM/egs_windows/egs_windows.html*," National Research Council Canada,
Accessed: 5/22/2007

[7] Walters, B., Kawrakow, I., Rogers, D. W. O., Ionizing Radiation Standards Group, "*DOSXYZnrc Users Manual: http:/www.irs.inms.nrc.ca/BEAM/user_manuals/ pirs794/pirs794.html*," National Research Council Canada, 2/13/2007.
Accessed: 5/22/2007

[8] Attix, F. H., *Introduction to Radiological Physics and Radiation Dosimetry*, WILEY-VCH Verlag GmbH & Co. KGaA, Weinheim, 2004.

[9] Cherry, S. R., Sorenson, J. A., Phelps, M. E., *Physics of Nuclear Medicine 3rd Edition*, Saunders / Elsevier, 2003.

[10] Karzmark, C. J., Morton, R. J., *A Primer on Theory and Operation of Linear Accelerators in Radiation Therapy*, Medical Physics Publishing, 1998.

[11] Chibani, O., Ma, C., *On the discrepancies between Monte Carlo dose calculations and measurements for the 18 MV Varian photon beam*, Med. Phys. 34 (4), April 2007.

[12] Jeraj, R., Keall, P. J., and Ostwald, P. M., "*Comparisons between MCNP, EGS4 and experiment for clinical electron beams*, Phys. Med. Biol. **44**, 1999.

[13] Seco, J., Evans, P. M., "*Assessing the effect on electron density in photon dose calculations*", Med. Phys. 33 (**2**), February, 2005.

[14] Wyatt, M. S., and Miller, L. F., "*A Comparison of Monte Carlo and Model-Based Dose Calculations in Radiotherapy using MCNPTV,*" Nuc. Inst. Meth. Phys. Res. A 1013-1016, 2006.

[15] X-5 Monte Carlo Team, "*MCNP-A General Monte Carlo N-Particle Transport Code, Version 5, Volume II: User's Guide*" Los Alamos Controlled Publication, April 24, 2003 (Revised 10/3/05).

[16] Verhaegen, F., and Seuntjens, J., "*Monte Carlo modeling of external radiotherapy photon beams,*" Phys. Med. Biol. **48** (2003) R107-R164.

[17] Lin, S. Y., Chu, T-C, and Lin J-P., "*Monte Carlo simulation of a clinical linear accelerator,*" Appl. Radiat. Isot. (**55**) 759-765, 2001.

[18] Van Laere, K. Mondelaers, W., "*Full Monte Carlo Simulation and Optimization of a High-Power Bremsstrahlung Converter,*" Radiat. Phys. Chem. (**49**), 207-219, 1997.

[19] Sheikh-Bagheri, D., Rogers, D. W. O., Ross, C. K., and Seuntjens, J. P., "*Comparison of Measured and Monte Carlo calculated dose distributions from the NRC linac*," Med. Phys 27 (10), October 2000.

[20] Lin S.-Y., Chu, T.-C., and Lin, J.-P., "*Monte Carlo Simulation of a Clinical Linear Accelerator*," App. Rad. Isot. (**55**), 7-59-765, 2001.

[21] Wang, B., Xu, G., Goorley, J. T., and Bozkurt, A., "*Issues Realted to the use of MCNP Code for an Extremely Large Voxel Model VIP-Man,*" American Nuclear Society Topical Meeting in Monte Carlo, Chattanooga, TN, 2005.